IEEE TRANSACTIONS ON MICROWAVE THEORY AND TECHNIQUES, VOL. MTT-34, NO. 6, JUNE 1986

Specific Absorption Rates of Energy in Man Models Exposed to Cellular UHF Mobile-Antenna Fields

ARTHUR W. GUY, FELLOW, IEEE, AND CHUNG-KWANG CHOU, MEMBER, IEEE

Abstract—Thermography, nonperturbing temperature probes, and *E*-field sensitive diodes were used to quantify the SAR patterns in human models exposed to UHF mobile-antenna fields. The exposure conditions include man, woman, and child models in the standing position close to roof- and trunk-mounted antennas; man sitting in the back seat near a trunk-mounted antenna; child kneeling in the back seat and looking through the rear window. Incident power densities near the antennas were also measured. Based on the current ANSI radio-frequency protection guide, the exemption of 7-W input power will violate the ANSI primary exposure criterion, but satisfies the 8-W/kg exclusion clauses. A maximum power of 3.5 W would satisfy all of the ANSI guides.

I. Introduction

THE POSSIBILITY of biological hazards from human exposure to electromagnetic radiation (EMR) has become a public concern in recent years. This concern has impacted the construction of new earth satellite communication antennas, terrestrial microwave links, and new broadcast antenna construction. Today, with the large number of vehicular mobile radios in service, and the expected increase of UHF mobile telephones in the future, one can expect that this new application of UHF energy will also be affected by the controversy. The first step in responding to such a potential impact is to determine whether there are any hazards to persons operating within the vicinity of such systems. For the health hazards of any electromagnetic source to be evaluated, it is necessary, first, to determine the amount of energy absorbed in the subjects from the source and, secondly, to determine from the literature on animal research whether any deleterious effects have occurred in test animals exposed at levels that produce the same amount of absorbed energy.

In this paper, we present our approach and results in determining the specific absorption rate (SAR) of energy with units of W/kg [1] in several full-sized human models exposed to ultra-high-frequency mobile-antenna fields. In brief, we determined the SAR by measuring the temperature rise in models, after a brief high-power exposure, with thermography [2] or with nonperturbing temperature probes. We also measured the induced electric fields in the model with diode sensors. The latter method has been used successfully by other authors for similar measurements in live animals [3] and phantom models exposed to various type sources [4], [5]. The measured level of exposure and energy absorption are compared to the values allowed by the current ANSI radio-frequency protection guide [6] in order to determine the safe operating conditions for the mobile communication system.

Manuscript received August 12, 1985; revised December 9, 1985.

A. W. Guy is with the Bioelectromagnetics Research Laboratory, University of Washington, Seattle, WA 98195.

C.-K. Chou is with the City of Hope Medical Center, Radiation Oncology Division, Duarte, CA 91010–0269.

IEEE Log Number 8607978.

II. Methods

A. Automobile and Exposure Chamber

A 1971 Mazda 1200 automobile body was chosen as the vehicle for testing the mobile antenna. The tests were conducted in a 12 ft × 12 ft × 24 ft anechoic chamber. The absorbing material on the floor in the shielded room was removed from the steel floor to simulate the most conductive ground condition.

B. Modification of Antennas

The original roof- and trunk-mounted antennas shown in Fig. 1, as supplied by Bell Laboratories, were designed for operation in the frequency range of 825–845 MHz with a low-power, 3- to 10-W mobile telephone system. In applying the thermographic technique, one must use considerably greater power than that used for operation of a mobile telephone system to heat the model during a very short exposure time. Since the original antennas could not handle such a high power, a different set of high-power antennas with the same radiation pattern as the original antennas had to be developed.

The roof-mounted antenna consisted of a half-wavelength antenna approximately 17.5 cm long with an 8-cm-long base coil mounted on an insulator designed to allow power to be fed through the roof of the automobile. The trunk-mounted antenna consisted of a similar radiator coil combination mounted on a 23-cm-high skirt.

For high-power operation, the roof-mounted antenna was simulated by a half-wavelength-long (18-cm) stub extension of the center conductor (dimensions given in Fig. 2(a)) of a standard EIA, $3\frac{1}{8}$ in-diameter coaxial line with a flange on the outer conductor designed to interface to the underside of the automobile roof. A slotted line was initially connected to the unmatched antenna for de-

0018-9480/86/0600-0671$01.00 ©1986 IEEE

Fig. 1. Original Bell Laboratories roof-mounted antenna (left) and trunk-mounted antenna (right).

termination of its input impedance. On the basis of the antenna-input impedance, a quarter-wave transformer was fabricated to match the antenna to the $3\frac{1}{8}$ in-diameter, 50-Ω EIA coaxial cable.

Upon completion of the antenna design, its performance in comparison to the original Bell Laboratories' antenna was evaluated. The performance of the high-power antennas was determined by terminating the identical receiving antenna with a 50-Ω load and energizing the transmitting antenna with 2–5 W of 835-MHz power. The distance between the receiving and transmitting antenna was 20 cm. A National Bureau of Standards (NBS) EDM-1C meter was set up with its sensor placed at 57.5 cm from the transmitting antenna. Measurements of power density were done for both the high-power antenna and the low-power Bell Laboratories' antennas; the results are shown in Table I. The measured values indicate that the performance characteristics of the antennas were similar.

A sketch of the high-powered trunk-mounted antenna is shown in Fig. 2(b). The antenna consisted of a nearly half-wavelength long stub section, similar to the roof-mounted antenna, protruding from a $3\frac{1}{8}$ in-diameter coaxial line containing a quarter-wave-shorted transmission-line skirt for decoupling the transmission line from the antenna. The quarter-wave transformer was used to match the impedance of the antenna to 50 Ω. The receiving antenna was mounted 115 cm away on the other side of the trunk.

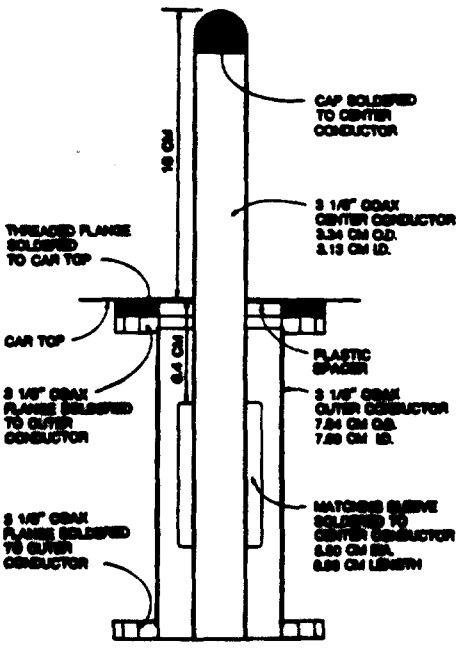

(a)

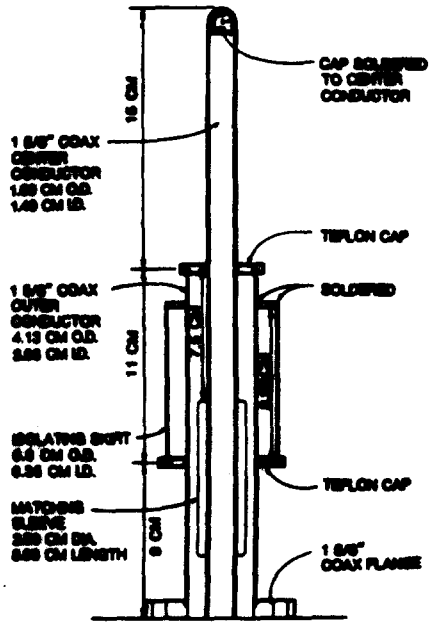

(b)

Fig. 2. (a) Sketch of high-power, 835-MHz, roof-mounted mobile antenna. (b) Schematic of high-power, 835-MHz, trunk-mounted antenna.

TABLE I
COMPARISON OF PERFORMANCE OF BELL LABORATORIES LOW-POWER, ROOF-MOUNTED ANTENNA WITH THAT OF HIGH-POWER ANTENNA

Antenna	Frwd. Pwr. (W)	Refl. Pwr. (W)	Net Pwr. (W)	NBS Meter Reading (mJ/m²)	Normal Pwr. Dens. (mW/cm² per Watt)
Bell Lab	2.51	0.128	2.39	1	0.088
	4.83	0.242	4.59	2	0.091
High Pwr.	2.53	0.022	2.51	1	0.084
	4.96	0.042	4.92	2	0.084

Location = Side of car, 2 cm below and 57.5 cm away from antenna tip
Frequency = 835-MHz

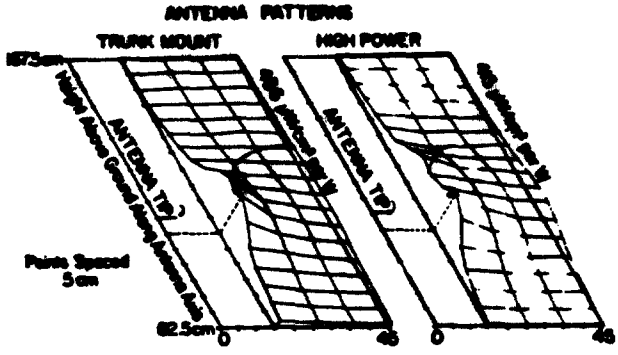

Fig. 3. Comparison of power-density patterns of Bell Laboratories' antenna and high-power trunk-mounted antenna.

A comparison of the patterns of the Bell Laboratories and the high-power trunk antennas are shown in Fig. 3. The power intensities were measured over distances of 15–45 cm from the antenna by means of the NBS EDM-1C energy density meter. To minimize the influence of instrumentation and the operator on the fields, absorbing materials were used to shield the meter and probe cable with the probe inserted through the absorbing material. The power density was measured in 5-cm increments vertically (1/7 wavelengths).

C. Phantom Models

The full-scale phantom models used in this research were of a man, a woman, and a child, and consisted of either hollow foam or fiberglass shells of human shape filled with synthetic gel having the same dielectric properties as human muscle. Though it has been demonstrated by other researchers that homogeneous whole-body phantom models with an electrical conductivity 2/3 that of muscle will provide the most realistic condition for determining whole body average SAR, this is not valid for local partial body exposures nor is it valid for determining SAR distribution within the model. No attempt was made to simulate skin, fat, bone, or internal organs. The styrofoam models used in the research were previously developed for a microwave-leakage study [7]. The woman model was designed to separate along a sagittal plane and also along a horizontal plane through the torso. The model corresponded to an adult female 1.63-m tall, weighing 59 kg. Another model

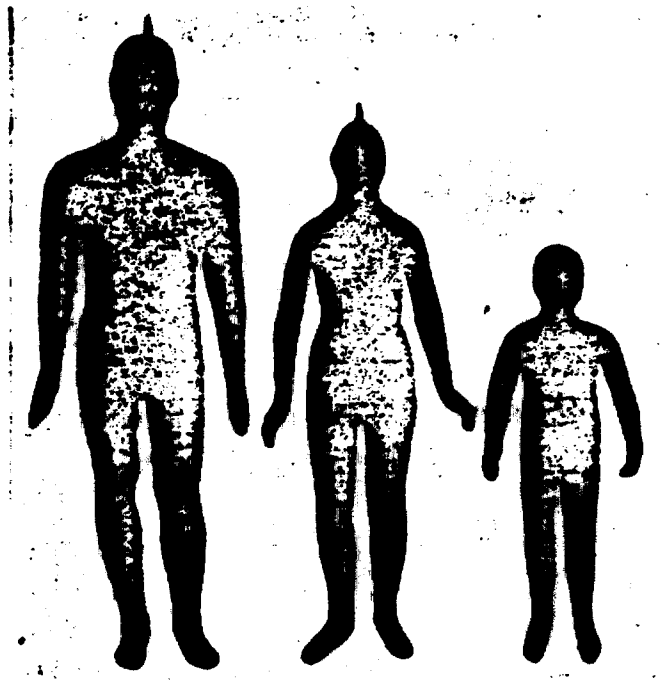

Fig. 4. Completed fiberglass shells with flanges at separation planes for man, woman, and child models.

simulated a child 94-m tall, weighing 15 kg. The models could also be sectioned transversely through the level of the eyes, where high SAR levels were expected for facial exposures. These models were used for measuring the SAR patterns in an adult female and a child exposed to the roof-mounted antenna fields, and a child exposed to the trunk-mounted antenna fields.

In addition to the foam models, hollow fiberglass models were formed by molding fiberglass material around commercial clothing store "mannequins." The hollow models were fabricated to represent a standing man and a sitting man. The hollow-fiberglass shells were bisected along the planes of interest, and flanges were attached to enable rapid assembly or disassembly of the model over the selected plane. The models simulating standing men, women, and children, are shown in Fig. 4.

With the fiberglass-shell models filled with synthetic muscle tissue, the weights and heights of the models were as follows: man 83.4 kg, 178 cm; woman 51.7 kg, 166 cm; and child 27.8 kg, 149 cm.

The phantom muscle consisted of 8.4454-percent TX150, 15.2027-percent polyethylene powder, 75.4445-percent water, and 0.9069-percent salt [2]. All percentages are by weight. The electrical and physical properties of the phantom muscle used to fill the shells of the model are shown in Table II. Prior to filling each half of a bisected model, each open shell at the plane of the bisection was covered with a 60-threads-per-in mesh, 7N6XX polyester silk screen (NBC Silk, Nagoya, Japan) stretched tightly over the flanges at the plane of separation. The model was then filled with the synthetic muscle through a hole at the top of the head of each half. The purpose of the silk screen was to ensure electrical contact between the halves of the model when

TABLE II
ELECTRICAL AND PHYSICAL PROPERTIES OF THE PHANTOM MUSCLE

	Dielectric constant ϵ	Conductivity σ (S/m)
Electrical properties (915 MHz)	51	1.24
	Specific heat (kcal/kg °C)	Specific density (g/cm^3)
Physical properties	0.86	0.97

Fig. 5. Erect man model separated along sagittal plane.

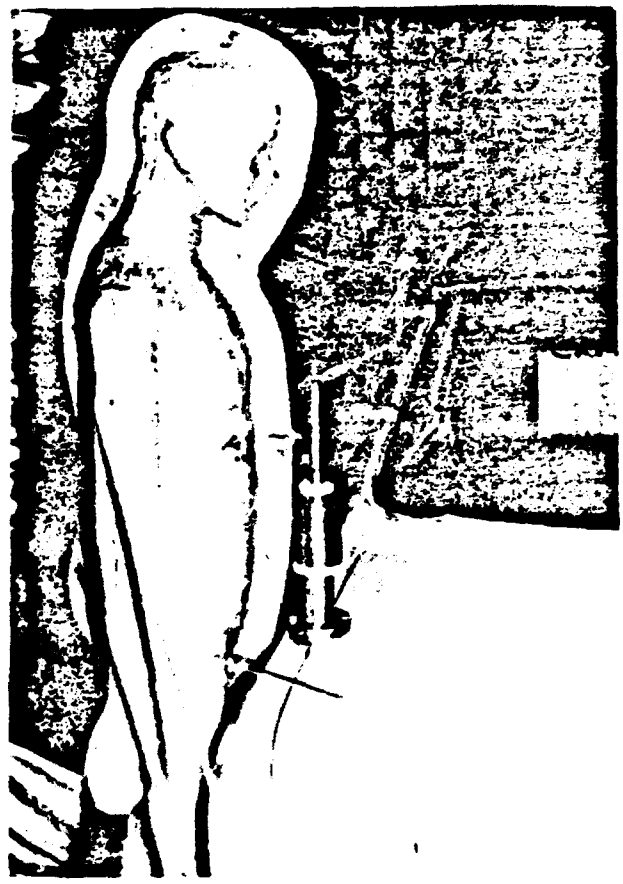

Fig. 6. Erect woman model exposed to trunk-mounted antenna.

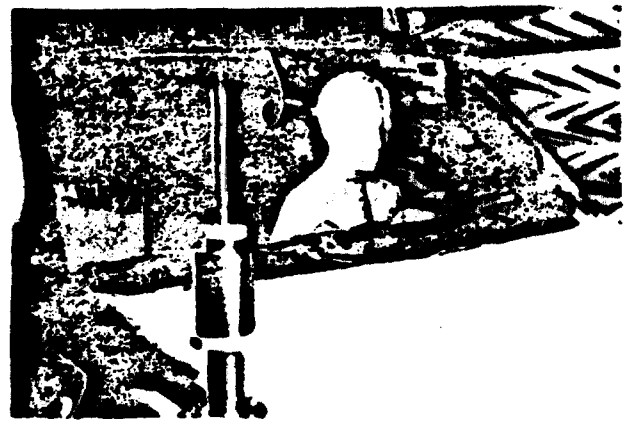

Fig. 7. Kneeling child model interior of automobile exposed to trunk mounted antenna.

they were joined and to allow easy separation of each half of the model along a smooth plane as shown in Fig. 5

D. Exposure Conditions

A number of possible exposure conditions were models in the study. Attempts were made to simulate worst-case exposure conditions resulting from the closest approaches of human subjects to the radiating antennas. These included man, woman, and child standing in close proximity to the side of the automobile near the trunk-mounted antenna as shown in Fig. 6, a man sitting in the back seat of the automobile, a woman standing near the rooftop-mounted antenna, a child held near the rooftop-mounted antenna and a child peering out the back window of the automobile (Fig. 7). In most instances, the subjects were exposed under conditions where 5- to 10-kW power was fed into the antennas from the traveling-wave-tube amplifier for periods of 20 to 90 s. In all exposure conditions, a high-powered load was placed at a feedpoint of the receiving antenna to absorb any of the power coupled to it from the transmitting antenna.

E. Measurement of Electromagnetic Fields In and Out of Automobile

In order to characterize the exposure field conditions, a number of electromagnetic field measurements using the

National Bureau of Standards EDM-1C energy-density meter were made. Measurements outside of the automobile were made at the sagittal plane of the model exposed to both the roof- and trunk-mounted antennas.

F. Measurement of SAR

Thermography: The thermographic method provides the most efficient way for establishing SAR over a two-dimensional internal plane within the exposed model. This method, described in detail elsewhere by Guy [2] and Guy *et al.* [7], is a valid for both far- and near-zone fields and involves the use of a thermographic camera for recording the temperature distributions produced by energy absorption in phantom models after exposure to radiation fields. The model was first disassembled along a plane where SAR was to be determined. A thermograph-temperature scan was then made over the plane. The model was then reassembled, exposed for a short time to high power density and then again disassembled, and another thermographic scan was made.

The thermographic method used in the past was first used for determination of the SAR in the foam woman and child models exposed to the roof-mounted antennas. A two-dimensional gray scale scan was immediately photographed after exposure of the model, and single *B*-scans with amplitude proportional to temperature were made before and after exposure. The two *B*-scans were photographed sequentially on the same film so that they were superimposed one upon the other as shown in Fig. 14 in Section III.

For later thermographic work with the trunk-mounted antenna, however, an improved thermographic technique was employed with digital recording and interactive-computer analysis. In general, whole-body thermograms were first taken over the bisected models for identification of regions of maximum SAR. Then a second series of thermographs were taken, in which the camera was moved closer to the object for better resolution of the regions where high SAR occurred.

Vitek 101 Temperature Probe: Since the thermographic measurements provided only the SAR at the bisected surfaces, the SAR's at other locations of the model had to be measured by other means. Four Vitek 101 temperature probes were used to measure the rate of temperature rise at four locations simultaneously. To minimize heat diffusion, the same high-power exposure technique that was used in the thermographic method was applied with an exposure period of about 1 min. The rate of temperature rise was recorded and theoretically converted to SAR at various points. In both man and woman models, the SAR's at the heart, kidney, liver, and stomach regions were measured. Since the breasts of the woman model were very close to the tip of the trunk-mounted antenna, the SAR in the center line of the breasts and 2.8 cm below the center line also were measured. For the child model, regions in the eyes, brain, and mouth were measured.

Electric-Field Probe: It was decided to use a Schottky diode of the type used for standard survey meters as a sensing element for measuring the weaker electric field within the model. An antenna was formed by encapsulating the diode in a conducting, bisecting pillbox (shown in Fig. 8) such that the bisected pillbox formed the poles of the receiving dipole. The diode was used to rectify the radiofrequency energy. High-resistance, small-diameter wires were used to carry the resulting rectified signal back to a meter. High sensitivity was obtained by modulation of the RF-source at 1000 Hz and use of a Hewlett–Packard 415E standing wave detector for sensing the 1000-Hz signal from the diode. The pillbox design shielded the loop formed by the high-resistance wire connections, preventing any induced voltages caused by magnetic fields.

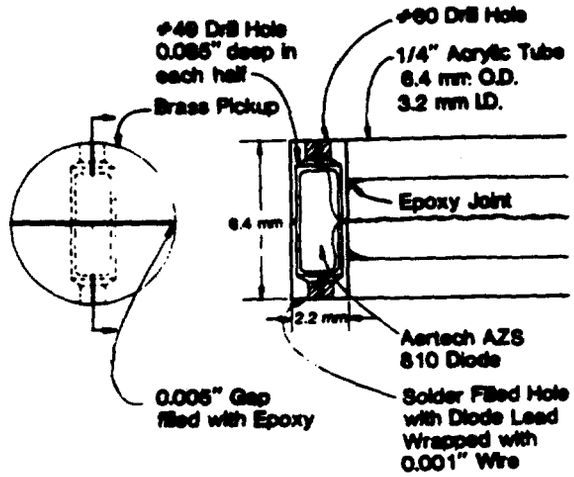

Fig. 8. Schematic of construction of diode probe for measuring electric-field strength.

The diode used was an Aertech AZS810. The high-resistance, twisted-pair, .001-in-diameter, .7-Ω-per-ft, nylon-coated resistance wire was protected from strain and mechanical damage by a $\frac{1}{4}$ in 30-cm-long acrylic tube. The high-resistance leads continued beyond the acrylic tube through a 90-cm-long, flexible plastic tubing. The twisted pair of leads were wrapped spirally around a $\frac{1}{16}$-in nylon catheter tube to take up any mechanical strain resulting from tension on the small twisted leads. At the end of the tubing, the twisted leads were connected to a standard RG58 shielded cable, which in turn was connected to the HP 415E standing wave detector.

The diode sensor was calibrated in a waveguide with its 24.8- × 12.4-cm cross section was loaded with a 11.6-cm-thick section of phantom muscle tissue. The fields in the phantom tissue were calculated by standard waveguide equations based on the input power.

III. Results

A. Field Mapping

The electric fields in the vicinity of each antenna were measured by means of an NBS EDM-1C electric-field energy density meter and converted to equivalent plane-wave power density. Fig. 9 illustrates the measurements with respect to the roof-mounted antenna in the sagittal plane of an exposed model. Fig. 10 illustrates similar

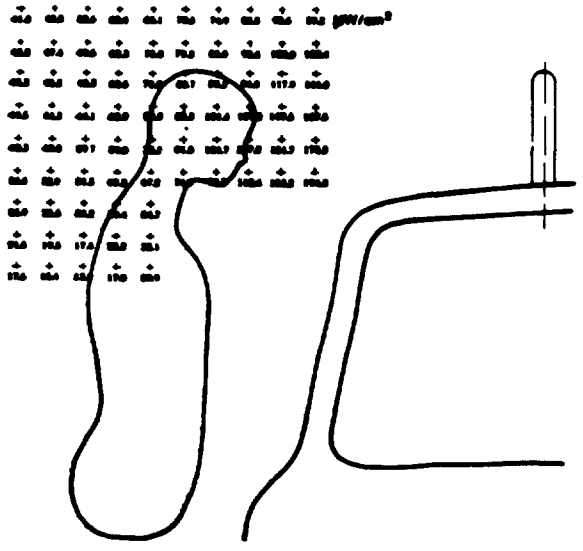

Fig. 9. Power densities due to 835-MHz radiation from roof-mounted antenna (input 1-W, outline for woman at 43.5 cm from antenna).

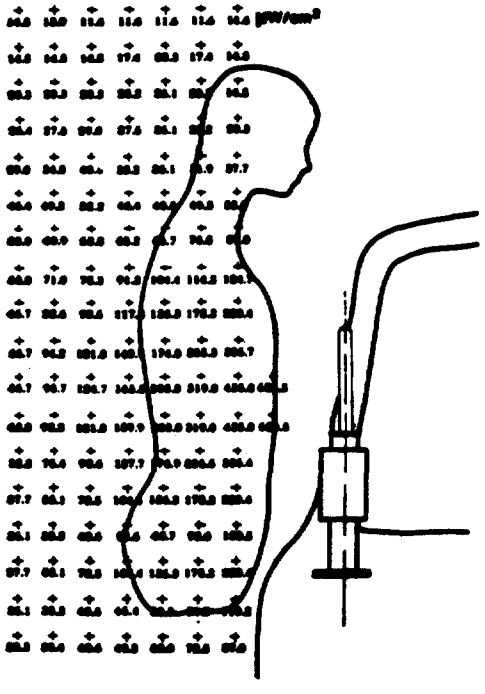

Fig. 10. Power densities from 835-MHz trunk-mounted antenna (1-W input power, outline of woman model standing 9.7 cm from antenna).

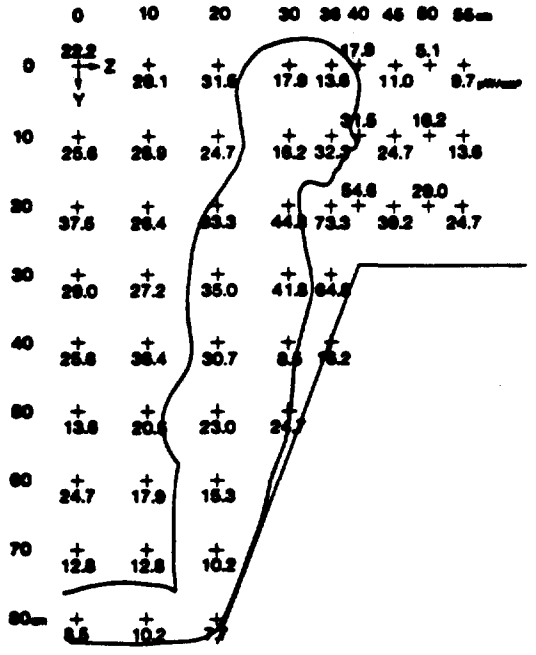

Fig. 11. Power densities due to 835-MHz radiation from trunk-mounted antenna (1-W input power, outline to child model).

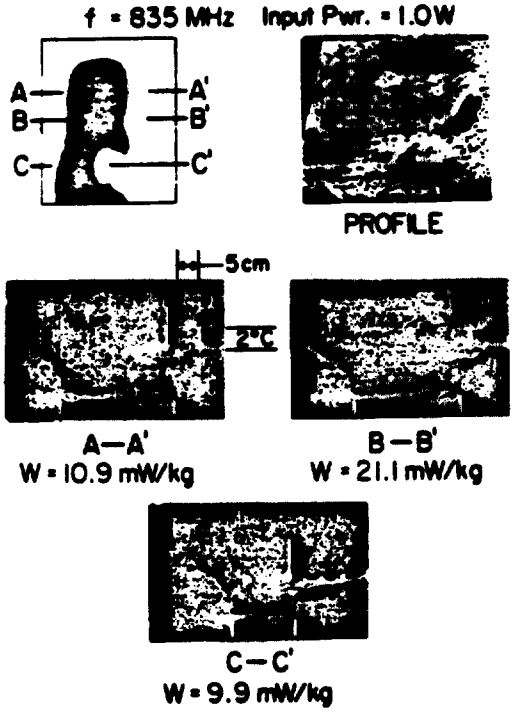

Fig. 12. Thermographically measured SAR patterns in woman model exposed 63 cm from roof-mounted antenna (sagittal plane).

measurements for the trunk-mounted antenna and Fig. 11 illustrates typical measurements made in the interior of the car near the rear window. The measurements are based on 1-W input to the transmitting antennas. The outline of the subjects are superimposed on the values of power density measured without the presence of the subject at the points designated by a + sign.

B. Thermography

Exposure of Subjects to Roof-Mounted Antenna: A typical thermograph scan for the exposure of the adult woman standing 63 cm from the roof-mounted antenna is shown in Fig. 12. The thermogram was taken of a sagittal scan through the head. The intensity scan (brightness proportional to temperature or SAR) is shown in the upper left of each figure. A profile scan with multiple scans with vertical deflections proportional to temperature of SAR is shown in the upper right of the figure. The lower three thermograms illustrated in the figure consists of *B*-scans taken before and after exposure along the lines $\underline{A-A'}$, $\underline{B-B'}$,

TABLE III(a)
SAR's IN CHILD MODEL EXPOSED TO ROOF-MOUNTED ANTENNA
(mW/kg/W)

		Eyes	Nose	Temple	
Horizontal plane at eye level	Standing straight (63 cm)	19.4 ± 2.6	17.4 ± 2.6	13.4 ± 0.8	
	Leaning forward (39 cm)	31.3 ± 2.7	36.0 ± 0.2	19.1 ± 3.5	
		Forehead	Nose	Mouth	Neck
Sagittal plane	Standing straight (63 cm)	5.0 ± 1.5	10.2 ± 1.7	4.0 ± 1.3	15.2 ± 1.9
	Leaning forward (39 cm)	21.6	52.7	16.1	27.5

TABLE III(b)
SAR's IN WOMAN MODEL EXPOSED TO ROOF-MOUNTED ANTENNA
(mW/kg/W)

		Eyes	Nose	Temple	
Horizontal plane at eye level	Standing straight (63 cm)	15.0 ± 0.8	17.0 ± 0.8	13	
	Leaning forward (43.5 cm)	35.0 ± 1.4	42.7 ± 1.9	36	
		Forehead	Nose	Mouth	Neck
Sagittal plane	Standing straight (63 cm)	11.5 ± 1.7	22.7 ± 1.3	13.7 ± 1.0	9.3 ± 1.2
	Leaning forward (43.5 cm)	14.4 ± 3.2	48.9 ± 9.4	20 ± 4.2	8.1 ± 1.3

$C - C'$ as noted on the intensity scan. The exposure time for these models was approximately 60 s. We determined the maximum SAR from the maximum temperature differences before and after exposure obtained from the double B-scans and the specific heat of the phantom tissue given in Table II. Since the SAR is proportional to the temperature differences denoted by the B-scans, one can easily visualize the SAR distribution from the vertical distance between these scans.

For the 63-cm-distance exposures the model was placed in a standing position, whereas for a closer position of 43.5 cm the model was allowed to lean toward the antenna at the closest possible distance. The maximum SAR's of 48.9 mW/kg/W for the leaning woman model and 22.7 mW/kg/W for the standing woman model occurred at the nose, as expected since it is the closest point of the body to the radiating antenna and it consists of wedge-shaped tissue, which allows greater energy disposition. Significant absorption was also found in the forehead, mouth, eye, temple, and neck. Based on the exposure levels given in Fig. 9, the maximum SAR varied from .3 to .44 W/kg per mW/cm^2 incident to the subject.

A series of thermographs were taken for a child model oriented 39 and 63 cm from the radiating antenna. At 39 cm, the child was assumed to be held by an adult as closely as possible to the antenna. Thermograms were taken for both the sagittal plane and the transverse plane cut through the orbital (eye) area of the child. The patterns for the child were similar to those of the woman, with maximum SAR levels reaching as high as 51.7 mW/kg/W input into the antenna of .35 W/kg per mW/cm^2 incident to the head of the child. Table III summarizes the maximum SAR's (Mean ± SD) in mW/kg/W input for both the child and the adult woman model exposed to the roof-mounted antenna for different regions of the body.

Exposure of Subjects to Trunk-Mounted Mobile Antenna: All thermography relating to the exposures of the models to the trunk-mounted antenna were recorded digitally and analyzed by a computer. In Fig. 13 are illustrated thermograms taken for the standing 0.94-m tall child model

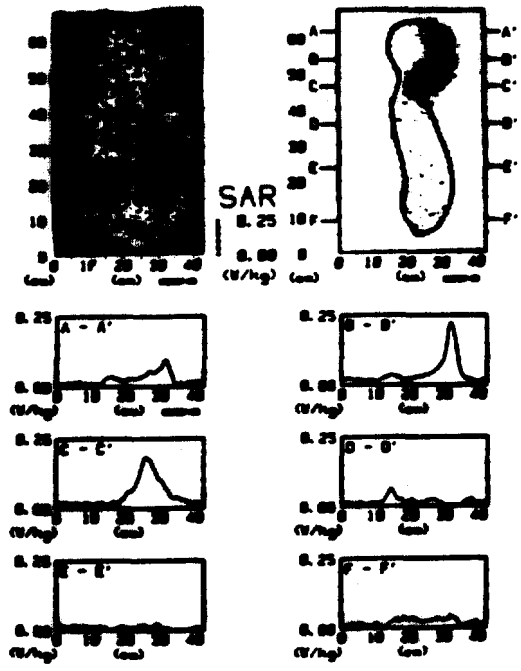

Fig. 13. Thermograms of SAR distribution in sagittal plane of child model, (1-W input, exterior exposure 15 cm from trunk-mounted antenna).

exposed with the head 15 cm from the trunk-mounted antenna. The figure at the upper-left-hand corner of the figure is a profile scan in which the horizontal scale corresponds to horizontal position and the left-hand scale corresponds to the vertical position. The vertical deflection of each scan is proportional to SAR with the values given by the SAR scale at the right of the figure. The display at the upper right-hand corner of the figure is an intensity scan in which the darkness is proportional to the SAR. The outline of the child is superimposed on the intensity scan. Single horizontal scans of SAR are shown at the lower half of the figure corresponding to the scan lines given in the upper right of the figure. The maximum SAR was found to be .23 W/kg/W input to the antenna. For the region of the eyes this corresponds to .64 W/kg per mW/cm^2 incident power density, based on the exposure levels in Fig. 10. Fig. 14 shows the close-up thermograms of the man model exposed to the trunk-mounted antenna at a 12-cm distance. The primary energy deposition was at the abdominal area at a maximum SAR of 0.12 W/kg/1W input at the surface. The SAR decreased exponentially as expected on a flat slab of tissue.

The fiberglass child model was the only model in which SAR distribution from exposure inside of the car was analyzed by thermography. For this series the model was designed to separate in the sagittal plane of the head and neck only. A maximum SAR in the vicinity of the orbital region of the eyes of .012 W/kg/W input to the antenna or approximately 0.32-W/kg per mW/cm^2 exposure level was obtained. In Table IV are illustrated the maximum SAR/W input to the antenna and maximum SAR per mW/cm^2 that were obtained thermographically for the various exposures from the trunk-mounted antennas.

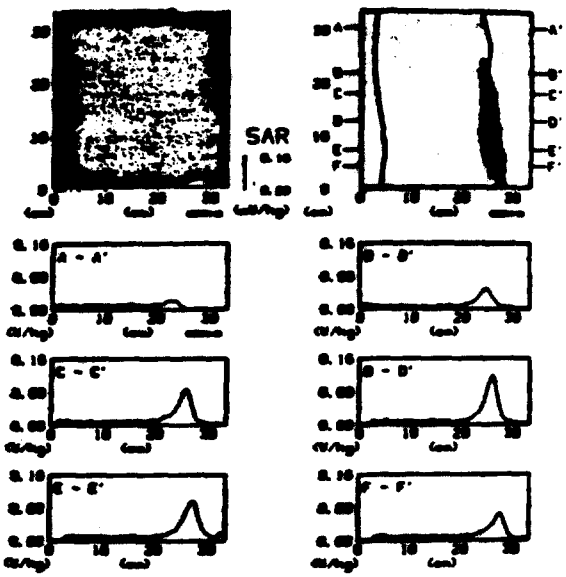

Fig. 14. Closeup thermograms showing SAR distribution in sagittal plane of man model exposed to 835-MHz in standing position exterior of automobile 12 cm from trunk-mounted antenna with 1-W input.

TABLE IV
MAXIMUM SAR'S (W/kg) IN MODELS EXPOSED TO TRUNK-MOUNTED ANTENNA

Model	Max. SAR per Watt	Max. SAR per mW/cm^2
Man outside	0.12	0.28
Woman outside	0.20	0.32
Child outside	0.23	0.64
Child inside	0.01	0.32

C. Vitek 101 Temperature Probe Data

In Tables V and VI are given the SAR data per 1-W power at various depths of the locations of the heart, kidney, liver, and stomach of the standing man and woman models exposed at 12 cm or 9.5 cm from the trunk-mounted antenna. The maximum level was at the stomach region in both models. The SAR's in the breast of the woman model are tabulated in Table VII; the values are smaller than those in the stomach and liver regions. In Table VIII are given the results for the child model.

D. Electric-Field Measurements in Subjects Exposed in Automobile

Fig. 15 illustrates the maximum SAR's measured at the surface of the face and neck of the child exposed in the automobile while looking out the back window. These measurements were made with the diode electric-field sensor inserted through the back of the head of the model, in contact with the internal surface of the fiberglass shell. The maximum level at the child model's nose is 60 percent higher than the maximum value obtained thermographically for the same model. However, thermographic values at other locations in the head were within 10 percent of values obtained by direct E-field measurements. The diffusion problem was worse for this case since an exposure

TABLE V
SAR'S OF STANDING MAN MODEL EXPOSED TO TRUNK-MOUNTED ANTENNA (W/kg/W)

Depth (cm)	Heart	Kidney	Liver	Stomach
1	0.0802	0.0316	0.1020	0.1320
2	0.0128	0.0148	0.0602	0.0832
3	0.0076	0.0081	0.0340	0.0425
4	0.0043	0.0046	0.0188	0.0204
5	0.0023	0.0023	0.0086	0.0089
6	0.0013	0.0013	0.0047	0.0037

TABLE VI
SAR'S OF STANDING WOMAN MODEL EXPOSED TO TRUNK-MOUNTED ANTENNA (W/kg/W)

Depth (cm)	Heart	Kidney	Liver	Stomach
0.5	0.0207	0.0746	0.117	0.147
1	0.0260	0.0642	0.110	0.135
2	0.0121	0.0307	0.0540	0.0727
3	0.0092	0.0171	0.0289	0.0381
4	0.0042	0.0074	0.0148	0.0189
5	0.0026	0.0034	0.0076	0.0084
6	0.0014	0.0025	0.0039	0.0040

TABLE VII
SAR'S IN BREAST OF STANDING WOMAN MODEL EXPOSED TO TRUNK-MOUNTED ANTENNA (W/kg/W)

Depth (cm)	Left (center)	Left (-2.8 cm)	Right (center)	Right (-2.8 cm)
0.5	0.0517	0.0788	0.0459	0.0864
1	0.0437	0.0843	0.0374	0.0742
2	0.0319	0.0353	[illegible]	[illegible]
3	0.0247	0.0283	[illegible]	0.0294
4	0.0180	0.0182	0.0181	0.0199
5	0.0133	0.0054	0.0130	0.0097
6	0.0079	0.0030	0.0074	0.0042
7	0.0040	0.0017	0.0035	0.0022
8	0.0022	0.0009	0.0015	[illegible]
9	0.0009	0.0005	0.0008	0.0004

TABLE VIII
SAR'S IN HEAD AND NECK OF STANDING CHILD EXPOSED TO TRUNK-MOUNTED ANTENNA (W/kg/W)

Depth (cm)	Eye Left	Eye Right	Nose Left	Nose Right	Mouth Right	Mouth Left
0	0.123	0.176	0.077	0.102	0.091	0.049
1.0	0.060	0.106	0.055	0.095	0.037	0.040
2.0	0.034	0.053	0.034	0.053	0.032	0.034
4.0	0.015	0.028	0.021	0.052	0.030	0.030
5.0	0.007	0.013	0.015	0.027	0.037	0.043
6.0	0.003	0.006	0.013	0.020	0.047	0.054
7.0					0.040	0.037
8.0					0.043	0.025
9.0					0.034	0.019
10.0					0.025	0.015
11.0					0.018	0.016
12.0					0.018	0.021
13.0					0.010	0.012

time exceeding two minutes was required to compensate for the sharp reduction of SAR from exposure within the automobile. The thermographic results can be expected to be lower as a result of reduction in temperature from thermal diffusion, especially in regions such as the nose prior to thermography. SAR's were also measured over the surfaces of the back of the head and neck of the man model sitting in the back of the car exposed to the trunk-

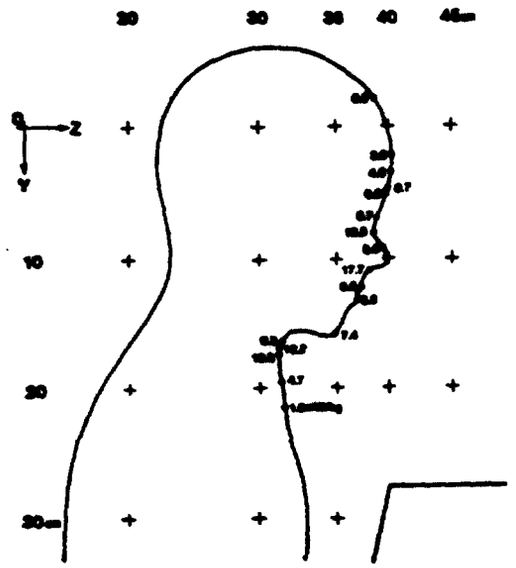

Fig. 15. SAR at the surface of the face of child model, 20 cm from trunk-mounted antenna with 1-W input power.

mounted antenna. The values were measured with the electric-field probe in the same manner as for the child. Maximum level at the neck of the man was 0.019 W/kg/W input into the antenna; this value corresponds approximately to .05 W/kg per mW/cm^2 of incident power density.

IV. Discussion

Table IX summarizes all of the results of the experimental measurements for maximum-power density and SAR per watt into the antenna and maximum SAR per mW/cm^2 incident to the subject for the various exposure conditions tried in this research. Application of the 0.4 W/kg ANSI exposure criteria based on a maximum whole-body exposure of 2.78 mW/cm^2 allowed for 835-MHz exposure would limit the input power to the antenna to 4.46 W for the condition resulting in the highest exposure level studied in this research (woman standing 9.7 cm from antenna). It is obvious, however, that under this restriction only a fraction of the 4.46 W emitted by the antenna would be absorbed by the exposed subject; thus, biologically the exposure level is much less significant than the same level for whole-body exposure. The RFPG takes into account such partial-body exposure conditions by specifying an exclusion clause that would allow higher exposure levels provided that the localized SAR in tissue does not exceed levels possible with plane-wave exposures at the recommended maximum power densities. This maximum level of SAR is 20 times the average, or 8 W/kg. Based on Table IX, this level of SAR would occur for the child standing 15 cm from the trunk-mounted antenna when an input power of 35 W was applied to the antenna.

In view of the fact that the highest levels of measured local SAR occurred in the region of the eyes of an exposed child 15 cm from the antenna, some comments should be made concerning possible microwave effects on the exposed eyes. The lowest thresholds for cataract formation in laboratory animals due to acute exposure to microwave radiation are more than 10 times above the maximum localized exposure and SAR levels allowed by the ANSI RFPG (requiring 50 to 100 min of exposure) at 150 to 500 mW/cm^2 corresponding to a localized SAR of 130 to 435 W/kg [9]–[11]. Also, it has been demonstrated that chronic exposure of rabbits for up to six months in duration to 10 mW/cm^2 maximum (SAR = 17 W/kg) failed to produce any cataracts [12]. It should be noted that the above experiments were conducted with rabbits whose eyes protrude from the head, and thus, are more susceptible to microwave damage. Similar experiments on monkeys, which more closely represent the human species, failed to produce cataracts at exposure levels as high as 150 to 500 mW/cm^2 [13], [14]. The ANSI RFPG and other forthcoming exposure guides exempt devices with less than 7-W input power to the antenna. The maximum power densities and SAR's for the worst-case exposure conditions tested with this input power to the antenna does not satisfy the ANSI primary exposure criteria; however, it does satisfy the 7-W and 8-W/kg exclusion clauses. On the other hand, a maximum input power of 3.5 W would satisfy all of the ANSI guides.

TABLE IX
Summary of Maximum Power Densities and SAR's for Various Exposure Conditions

[illegible]	[illegible]	[illegible]	[illegible]	[illegible]	[illegible]
[illegible]	[illegible]	[illegible]	[illegible]	[illegible]	[illegible]
[illegible]	[illegible]	[illegible]	[illegible]	[illegible]	[illegible]
[illegible]	[illegible]	[illegible]	[illegible]	[illegible]	[illegible]
[illegible]	[illegible]	[illegible]	[illegible]	[illegible]	[illegible]
[illegible]	[illegible]	[illegible]	[illegible]	[illegible]	[illegible]
[illegible]	[illegible]	[illegible]	[illegible]	[illegible]	[illegible]
[illegible]	[illegible]	[illegible]	[illegible]	[illegible]	[illegible]
[illegible]	[illegible]	[illegible]	[illegible]	[illegible]	[illegible]
[illegible]	[illegible]	[illegible]	[illegible]	[illegible]	[illegible]
[illegible]	[illegible]	[illegible]	[illegible]	[illegible]	[illegible]
[illegible]	[illegible]	[illegible]	[illegible]	[illegible]	[illegible]
[illegible]	[illegible]	[illegible]	[illegible]	[illegible]	[illegible]
[illegible]	[illegible]	[illegible]	[illegible]	[illegible]	[illegible]

We may conclude from the results that the mobile-antenna system can be operated safely with all of the ANSI RFPG exposure guides in terms of both power density and maximum SAR for input powers of 3.5 W or less and within the guidelines of the ANSI exclusion clause for input powers up to 35 W. Furthermore, on the basis of average power density for the brief transmission periods in which persons may be exposed under the conditions studied in this research, operation of the antenna is not likely to result in emissions that exceed some of the newly proposed general population standards now being proposed by various government agencies for different tissue types and structures.

It has been shown that the experimental methods used in this research can adequately quantify both maximum exposure levels and SAR's for subjects exposed in the near-field of UHF mobile transmitting antennas. These techniques also can be applied equally well to other exposure conditions, involving fixed portable and mobile antennas and radiation devices operating at other frequencies. It appears that the methodology would be most useful in determining whether certain types of radiating devices could meet the ANSI 0.4-W/kg average and 8.0-W/kg maximum SAR exclusion clause. The models used in this research were simple, homogeneous figures, but there are

no technical restrictions in fabricating more advanced and realistic designs.

References

[1] NCRP Report No. 67, "Radiofrequency electromagnetic fields properties, quantities and units, biophysical interaction, and measurements," Nat. Council on Radiation Protection and Measurements, Washington, DC, Mar. 1, 1981.

[2] A. W. Guy, "Analysis of electromagnetic fields induced in biological tissues by thermographic studies on equivalent phantom models," *IEEE Trans. Microwave Theory Tech.*, vol. MTT-19, pp. 205–214, Feb. 1971.

[3] C. C. Johnson and A. W. Guy, "Nonionizing electromagnetics wave effects in biological materials and systems," *Proc. IEEE*, vol. 60, pp. 692–718, June 1972.

[4] S. S. Stuchly, A. Kraszewski, M. A. Stuchly, G. Hartsgrove, and D. Adamski, "Energy deposition in a model of man in the near field," *Bioelectromagnetics*, vol. 6, no. 2, pp. 115–129, 1985.

[5] A. Kraszewski, M. A. Stuchly, S. S. Stuchly, G. Hartsgrove, and D. Adamski, "Specific absorption rate distribution in a full-scale model of man at 350 MHz," *IEEE Trans. Microwave Theory Tech.*, vol. MTT-32, pp. 779–783, Aug. 1984.

[6] ANSI, "American national standard safety levels with respect to human exposure to radio frequency electromagnetic fields, 300 kHz to 100 GHz," IEEE, 1982.

[7] M. D. Webb, A. W. Guy, and J. A. McDougall, "Assessment of EM-field coupling of 915-MHz oven-door leakage to human subjects by thermographic studies on phantom models," *J. Microwave Power*, vol. 11, pp. 162–164, 1976.

[8] A. W. Guy, M. D. Webb, and C. Sarason, "Determination of power absorption in man exposed to high-frequency electromagnetic fields by thermograph measurements on scale models," *IEEE Trans. Biomed. Eng.*, vol. BME-23, no. 5, pp. 361–371, Sept. 1976.

[9] R. Carpenter, E. Ferri, and G. Hagen, "Assessing microwaves as a hazard to the eye—progress and problems," in *Proc. Int. Symp. Bio. Effects Health Hazards Microwave Radiation*, (Warsaw) Polish Medical Publishers, pp. 178–185, 1974.

[10] A. W. Guy, J. Lin, P. Kramar, and A. Emery, "Effect of 2450-MHz radiation on the rabbit eye," *IEEE Trans. Microwave Theory Tech.*, vol. MTT-23, pp. 492–498, June 1975.

[11] P. O. Kramar, A. Emery, A. W. Guy, and J. Lin, "The ocular effects of microwaves on hyperthermic rabbits: A study of microwave cataractogenic mechanisms," *Ann. NY Acad. Sci.*, vol. 247, pp. 155–165, Feb. 1975.

[12] A. W. Guy, P. O. Kramar, C. A. Harris, C. K. Chou, "Long term 2450-MHz CW microwave irradiation of rabbits," *J. Microwave Power*, vol. 15, no. 1, pp. 37–44, 1980.

[13] P. Kramar, C. Harris, A. F. Emery, and A. W. Guy, "Acute microwave irradiation and cataract formation in rabbits and monkeys," *J. Microwave Power*, vol. 13, pp. 240–249, 1978.

[14] R. D. McAfee, A. Longacre, Jr., R. R. Bishop, S. T. Elder, J. G. May, M. G. Holland, and R. Gordon, "Absence of ocular pathology after repeated exposure of unanesthetized monkeys to 9.3-GHz microwaves," *J. Microwave Power*, vol. 14, no. 1, pp. 41–44, Mar. 1979.

Arthur W. Guy (S'54–M'57–SM'74–F'77) was born in Helena, MT, on December 10, 1928. He received the B.S. degree in 1955, the M.S. degree in 1957, and the Ph.D. degree in 1966, all in electrical engineering from the University of Washington, Seattle.

From 1947 to 1950 and from 1951 to 1952, he served in the U.S. Air Force as an Electronic's Technician. Between 1957 and 1964, he was a Research Engineer in the Antenna Research Group, Boeing Aerospace Company, Seattle. While there, his field included research on broad-band and microwave devices, surface wave antennas, propagation through anisotrophic dielectrics, and antennas buried in lossy media. Between 1964 and 1966, he was employed by the Department of Electrical Engineering, University of Washington, conducting research on VLF antennas buried in polar ice caps. At that time, he also served as Consultant to the Department of Rehabilitation Medicine, working on problems associated with the effect of electromagnetic fields on living tissue. In 1966, he joined the faculty in the Department of Rehabilitation Medicine. Presently, he is a Professor in the Center for Bioengineering, has a joint appointment as Professor in Rehabilitation Medicine and Adjunct Professor in Electrical Engineering. Dr. Guy is Director of the Bioelectromagnetics Research Laboratory in the Bioengineering Center and is involved in teaching and research in the area of biological effects and medical applications of electromagnetic energy. He is a member of the AAAS, Bioelectromagnetics Society, the IEEE ANSI C95 Committee, ANSI C95.4 Subcommittee, and was Chairman of the 1970-1982 Subcommittee IV that developed the protection guides for human exposures to radiofrequency fields in 1974 and 1982. He is a member of NCRP, and Chairman of the Scientific Committee 53 responsible for biological effects and exposure criteria for radiofrequency fields, COMAR Commission A, and was a member of the EPA Scientific Advisory Board Ad Hoc Committee on Biological Effects of Radiofrequency Fields. Dr. Guy also serves as a consultant of the NIEHS on the USSR-US Environmental Health Cooperative Program and was a member of the NIH Diagnostic Radiology Study Section 1979-1983. Dr. Guy is a member of the editorial boards of the Journal of Microwave Power and IEEE Transactions on Microwave Theory and Techniques and is Past-President of the Bioelectromagnetics Society.

Dr. Guy holds memberships in Phi Beta Kappa, Tau Beta Pi, and Sigma Xi.

Chung-Kwang Chou (S'72–M'75) was born in Chung-King, China, on May 11, 1947. He received the B.S. degree from the National Taiwan University in 1968, the M.S. degree from Washington University, St. Louis, MO, in 1971, and the Ph.D. degree from the University of Washington, Seattle, in 1975, all in electrical engineering.

During his graduate study at the University of Washington, Dr. Chou had extensive training in both electromagnetics and physiology. He spent a year as an NIH postdoctoral fellow in the Regional Primate Research Center and the Department of Physiology and Biophysics at the University of Washington. He was a Research Associate Professor in the Center for Bioengineering and the Department of Rehabilitation Medicine, as well as Associate Director of the Bioelectromagnetics Research Laboratory until August 1985, engaged in teaching and research in electromagnetic dosimetry, exposure systems, biological effects of microwave exposure, and RF hyperthermia for cancer treatment. Dr. Chou now is the head of the Biomedical Engineering Section of the Department of Radiation Research at the City of Hope National Medical Center, Duarte, CA. His main research is in cancer hyperthermia. A consultant for the NCRP's scientific committee 53 on the biological effects and exposure criteria for radio-frequency electromagnetic fields, Dr. Chou has also served on the ANSI Subcommittee C95.4 since 1978, and is now the chairman of the 3-kHz–3-MHz working group. He was the chapter chairman of IEEE's Seattle Section on Antennas and Propagation/Microwave Theory and Technique in 1981–1982. Dr. Chou was on the Board of Directors of the Bioelectromagnetics Society and is on the editorial board of the Journal of Bioelectromagnetics. He is also a member of the Bioelectromagnetics peer review group of the American Institute of Biological Sciences and BEMS, AAAS, IMPI, the Radiation Research Society, Tau Beta Pi, and Sigma Xi.

In 1981, Dr. Chou received the first special award for the decade of the 70's from the International Microwave Power Institute for contributions in medical and biological research.

SPECIFIC ABSORPTION RATES OF ENERGY IN MAN MODELS EXPOSED TO UHF-MOBILE-ANTENNA FIELDS

Arthur W. Guy, Ph.D.
Chung-Kwang Chou, Ph.D.
Carrol Sorensen
John A. McDougall, B.S.
Gen-Yuan Yang, B.S.
Donald Reynolds, Ph.D.

Bioelectromagnetics Research Laboratory
Department of Rehabilitation Medicine
Center for Bioengineering
Department of Electrical Engineering
School of Medicine
and
College of Engineering
University of Washington
Seattle, Washington

Scientific Report No. 25
May 1983

Final Report

Prepared for
Bell Laboratories
Murray Hill, New Jersey 07974

TABLE OF CONTENTS

	Page
LIST OF TABLES	1
LIST OF FIGURES	3
1 INTRODUCTION	8
Problem	8
Solution	8
2 TECHNICAL APPROACH	11
Automobile-Exposure Chamber and Radio Frequency Source	11
Modification of Antennas	16
Phantom Models	21
Exposure Conditions	32
Measurement of Electromagnetic Fields in and out of Automobile	41
Measurement of SAR	41
Thermography	41
Vitek 101 Temperature Probe	46
Electric Field Probe	49
3 EXPERIMENTAL RESULTS	59
Field Mapping	59
Thermography	70
Exposure of Subjects to Roof-Mounted Mobile Antenna	70
Exposure of Subjects to Trunk-Mounted Mobile Antenna	79
Exposure to Fields inside Car from Trunk-Mounted Antenna	86
Vitek 101 Temperature Probe Data	86
Electric-Field Measurements in Subjects Exposed in Automobile	95
4 CONCLUSIONS AND FUTURE RESEARCH	101
REFERENCES	111
APPENDIX A. COMPUTERIZED THERMOGRAPHIC SYSTEM	A1

LIST OF TABLES

Table 1. Comparison of performance of Bell Laboratories low-power, roof-mounted antenna with that of high-power antenna.

Table 2. Composition and electrical and physical properties of the phantom muscle.

Table 3a. Values for electric field strength, apparent power density, actual power density and SAR along axis of waveguide as function of distance from muscle Eccofoam slab interface, waveguide with dimensions 12.4 cm by 24.68 cm, with 1-W input power. Dielectric constant of muscle = 50.6 -j.266.

Table 3b. Values for electric field strength, apparent power density, actual power density and SAR along axis of waveguide as function of distance from muscle Eccofoam slab interface, waveguide with dimensions 12.4 cm by 24.68 cm, with 1-W input power. Dielectric constant of muscle = 50.6 -j.266.

Table 4. Comparison of measurements of power density made with NBS EDM-1C and Holaday 3001 survey meters at 835-MHz, with 1-W input to source.

Table 5a. SARs in woman model exposed to roof-mounted antenna (mW/kg per watt).

Table 5b. SARs in child model exposed to roof-mounted antenna (mW/kg per watt).

Table 6. Maximum SARs in models exposed to trunk-mounted antenna.

Table 7. SARs of standing man model exposed to trunk-mounted antenna (W/kg per watt).

Table 8. SARs of standing woman model exposed to trunk-mounted antenna (W/kg per watt).

Table 9. SARs in breast of standing woman model exposed to trunk-mounted antenna.

Table 10. SARs in head and neck of standing child exposed to trunk-mounted antenna (W/kg per watt).

Table 11. Summary of maximum power densities and SARs for various exposure conditions.

Table 12. Maximum input powers into antenna allowed by the ANSI C95.1, 1982 standard for various exposure conditions.

Table 13. Summary of maximum power densities and SARs corresponding to 7-W input power to antenna for various exposure conditions.

Table 14. Summary of maximum power densities and SARs corresponding to 3.5-W input power to antenna for various exposure conditions.

Table 15. Electromagnetic fields and equivalent power densities of ideal dipole antenna, freq = 835.00 MHz, height or 1/2 length = 0.25 wavelengths, input resistance = 72.00 OHMS, input power = 7.00 watts, grid size = 0.10 m, origin (0.00,0.00).

Table 16. Electromagnetic fields and equivalent power densities of ideal dipole antenna, freq = 835.00 MHz, height or 1/2 length = 0.25 wavelengths, input resistance = 72.00 OHMS, input power = 7.00 watts, grid size = 0.05 m, origin (0.00, 0.00).

Table 17. Electromagnetic fields and equivalent power densities of ideal dipole antenna, freq = 835.00 MHz, height or 1/2 length = 0.25 wavelengths, input resistance = 72.00 OHMS, input power = 3.50 watts, grid size = 0.10 m, origin (0.00, 0.00).

Table 18. Electromagnetic fields and equivalent power densities of ideal dipole antenna, freq = 835.00 MHz, height or 1/2 length = 0.25 wavelengths, input resistance = 72.00 OHMS, input power = 3.50 watts, grid size = 0.05 m, origin (0.00, 0.00).

Table 19. Comparison of measured maximum power densities from mobile antenna with calculated maximum theoretical values from half-wavelength-long dipole with 1-W input to antenna.

LIST OF FIGURES

Fig. 1. Modification of automobile body for UHF antenna tests.

Fig. 2. Schematic of BEMRL anechoic exposure chamber.

Fig. 3. Original Bell Laboratories roof-mounted antenna (left) and trunk-mounted antenna (right).

Fig. 4. Test automobile body in anechoic chamber with roof-mounted receiving and transmitting antennas (technician is measuring antenna VSWR with slotted line).

Fig. 5. Photograph of 10-kW klystron amplifier with excitation signal generator, amplifier, liquid-dummy load control system, output power meter and reflected power meter.

Fig. 6. High-power, roof-mounted antenna and slotted line for measuring impedance.

Fig. 7a. Sketch of high-power, 835-MHz, roof-mounted mobile antenna.

Fig. 7b. Photograph of center conductor with quarter-wave matching transformer.

Fig. 8. Measurement of performance of high-power, roof-mounted antenna with National Bureau of Standards EDM-1C energy density meter.

Fig. 9a. Schematic of high-power, 835-MHz, trunk mounted antenna.

Fig. 9b. Photograph of high-power, trunk-mounted antenna and EDM-1C energy-density probe for measuring antenna fields.

Fig. 10. Comparison of power-density patterns of Bell Laboratories antenna and high-power trunk mounted antenna.

Fig. 11. Foam shells used for fabricating woman models, designed for separation along sagittal plane and horizontal plane through torso.

Fig. 12. Foam child model filled with synthetic muscle and separated along sagittal plane.

Fig. 13. Construction of fiberglass shell for phantom model of erect man.

Fig. 14. Fiberglass shell for phantom model of sitting man.

Fig. 15. Completed fiberglass shells with flanges at separation planes for man, woman, and child models. Woman model covered with metal foil shows applicability of models for measuring body currents due to exposure to electric fields at ELF through medium-frequency range.

Fig. 16. Erect man model separated along sagittal plane.

Fig. 17. Woman model (separated along sagittal plane for illustration) exposed to roof-mounted mobile antenna.

Fig. 18. Child model exposed to roof-mounted antenna (carried position).

Fig. 19. Erect child model exposed to trunk-mounted antenna.

Fig. 20. Erect woman model exposed to trunk-mounted antenna.

Fig. 21. Erect man model exposed to trunk-mounted antenna.

Fig. 22. Sitting man model in back seat of automobile exposed to trunk-mounted antenna.

Fig. 23. Kneeling child model interior of automobile exposed to trunk-mounted antenna.

Fig. 24. Measurement of power-density pattern in vicinity of trunk-mounted antenna with EDM-1C survey meter.

Fig. 25. Arrangement of EDM-1C meter probe for measuring power density pattern in interior of automobile due to emission from trunk-mounted antenna.

Fig. 26. Separation along orbital plane of phantom child model exposed to roof-mounted antenna.

Fig. 27. Thermograph scanning orbital plane of phantom child model.

Fig. 28. Method of separating parts of kneeling child model for determination of SAR in sagittal plane of head.

Fig. 29. Four Vitek 101 temperature probes for measuring simultaneously SAR in man model at four locations.

Fig. 30. Photograph showing Schottky diode, bisected pillbox dipole, and twisted-pair leads before assembly.

Fig. 31. Schematic of construction of diode probe for measuring electric-field strength.

Fig. 31. (continued) Schematic of construction of diode probe for measuring electric-field strength.

Fig. 32. Photograph of diode for measuring electric-field strength, cable, and HP 415E meter.

Fig. 33. Block diagram of equipment used for calibration of probe for measuring electric-field strength.

Fig. 34. Power densities exterior of automobile due to 835-MHz radiation from roof-mounted antenna, with 1-W input power (outline shows position of exposed woman model standing 43.5 cm from antenna).

Fig. 35. Power densities exterior of automobile due to 835-MHz radiation from roof-mounted antenna, with 1-W input power (outline shows position of exposed woman model standing 63 cm from antenna).

Fig. 36. Power densities exterior of automobile due to 835-MHz radiation from roof-mounted antenna, with 1-W input power (outline shows position of exposed child model held 39 cm from antenna).

Fig. 37. Power densities exterior of automobile due to 835-MHz radiation from roof-mounted antenna, with 1-W input power (outline shows position of exposed child model held 63 cm from antenna).

Fig. 38. Power densities exterior of automobile due to 835-MHz radiation from trunk-mounted antenna, with 1-W input power (outline shows position of exposed man model standing 12 cm from antenna).

Fig. 39. Power densities exterior of automobile due to 835-MHz radiation from trunk-mounted antenna with 1-W input power (outline shows position of exposed woman model standing 9.7 cm from antenna).

Fig. 40. Power densities exterior of automobile due to 835-MHz radiation from trunk-mounted antenna with 1-W input power (outline shows position of exposed child model standing 15 cm from antenna).

Fig. 41. Region in autombile (Y-Z plane) where power densities due to 835-MHz radiation from trunk-mounted antenna were measured (each intersection of dashed lines corresponds to measurement point).

Fig. 42. Region in automobile (X-Y plane) where power density due to 835-MHz radiation from trunk-mounted antenna were measured (each intersection of dashed lines corresponds to measurement point).

Fig. 43. Position of sitting man model interior of automobile exposed to 835-MHz radiation from trunk-mounted antenna with 1-W input power (Y-Z plane, X= 30cm).

Fig. 44. Position of sitting man model interior of automobile exposed to 835-MHz radiation from trunk-mounted antenna with 1-W input power (X-Y plane, Z= 30 cm).

Fig. 45. Position of kneeling child model interior of automobile exposed to 835-MHz radiation from trunk-mounted antenna with 1-W input power (Y-Z plane, X= 20 cm).

Fig. 46. Position of kneeling child model interior of automobile exposed to 835-MHz radiation from trunk-mounted antenna with 1-W input power (X-Y plane, Z= 30 cm).

Fig. 47. Thermographically measured SAR patterns in woman model exposed 43.5 cm from roof-mounted antenna (sagittal plane).

Fig. 48. Thermographically measured SAR patterns in woman model exposed 43.5 cm from roof-mounted antenna (transverse plane through eyes).

Fig. 49. Thermographically measured SAR patterns in woman model exposed 63 cm from roof-mounted antenna (sagittal plane).

Fig. 50. Thermographically measured SAR patterns in woman model exposed 63 cm from roof-mounted antenna (transverse plane).

Fig. 51. Thermographically measured SAR patterns in child model exposed 39 cm from roof-mounted antenna (sagittal plane).

Fig. 52. Thermographically measured SAR patterns in child model exposed to 39 cm from roof-mounted antenna (transverse plane through eyes).

Fig. 53. Thermographically measured SAR patterns in child model exposed 63 cm from roof-mounted antenna (sagittal plane).

Fig. 54. Thermographically measured SAR patterns in child model exposed 63 cm from roof-mounted antenna (transverse plane).

Fig. 55. Computer-processed thermograms showing SAR distribution in sagittal plane of man model exposed to 835-MHz in standing position exterior of automobile 12 cm from trunk-mounted antenna with 1-W input.

Fig. 56. Closeup thermograms showing SAR distribution in sagittal plane of man model exposed to 835-MHz in standing position exterior of automobile 12 cm from trunk-mounted antenna with 1-W input.

Fig. 57. Computer-processed thermograms showing SAR distribution in sagittal plane of woman model exposed to 835-MHz in standing position exterior of automobile 9.7 cm from trunk-mounted antenna with 1-W input.

Fig. 58. Closeup thermograms showing SAR distribution in sagittal plane of woman model exposed to 835-MHz in standing position exterior of automobile 9.7 cm from trunk-mounted antenna with 1-W input.

Fig. 59. Computer-processed thermograms showing SAR distribution in sagittal plane of child model exposed to 835-MHz in standing position exterior of automobile 15 cm from trunk-mounted antenna with 1-W input.

Fig. 60. Closeup thermograms showing SAR distribution in sagittal plane of child model exposed to 835-MHz in standing position exterior of automobile 20 cm from trunk-mounted antenna with 1-W input.

Fig. 61. Computer-processed thermograms showing SAR distribution in sagittal plane of child model exposed to 835-MHz in kneeling position interior of automobile 20 cm from trunk-mounted antenna with 1-W input.

Fig. 62. Closeup thermograms showing SAR distribution in sagittal plane of child model exposed to 835-MHz in kneeling position interior of automobile 70 cm from trunk-mounted antenna with 1-W input.

Fig. 63. Maximum SAR at the surface of the face of child model in kneeling position interior of automobile exposed to 835-MHz radiation from trunk-mounted antenna with 1-W input power (Y-Z plane, X= +20 cm).

Fig. 64. Maximum SARs at the surfaces of the eye, neck, and forehead of child model in kneeling position interior of automobile exposed to 835-MHz radiation from trunk-mounted antenna with 1-W input power (X-Y plane, Z= 30 cm).

Fig. 65. Maximum SAR at the back of head surface of man model in sitting position interior of automobile exposed to 835-MHz radiation from trunk-mounted antenna with 1-W input power (Y-Z plane, X= +30 cm).

Fig. 66. Maximum SARs at the back of head, and shoulder and neck surfaces of man model in sitting position interior of automobile exposed to 835-MHz radiation from trunk-mounted antenna with 1-W input power (X-Y plane, Z= 30 cm).

SPECIFIC ABSORPTION RATES OF ENERGY IN MAN MODELS EXPOSED TO UHF-MOBILE-ANTENNA FIELDS

1 INTRODUCTION

Problem

The possibility of biological hazards from human exposure to electromagnetic radiation (EMR) has become a public concern in recent years. Today, approximately 160,000 vehicular mobile radios are currently in service, and with the expected increase of UHF mobile telephones in the future, it is important to determine whether there are any hazards to persons operating in or in the vicinity of such systems. For the health hazards of any electromagnetic source to be evaluated, it is necessary, first, to determine the amount of energy absorbed in the subjects from the source and, secondly, to determine from the literature on animal research whether any deleterious effects have occurred in test animals exposed at levels that produce the same amount of absorbed energy. No measured data are available in the literature concerning energy coupling between nonuniform, near-zone fields of cellular radio mobile antennas and exposed simulated human subjects.

Solution

There are several approaches for determining the amount of energy absorbed in a subject exposed to mobile UHF antennas. One method developed by Guy (1971) enables rapid evaluation of specific absorption rate (SAR) of energy in tissues of arbitrary shapes when they are exposed to various electromagnetic sources. This method, valid for both far- and near-zone fields, involves the use of an infrared thermograph camera for recording temperature distribution produced by energy absorption in phantom models of human subjects. The SAR may be obtained anywhere in the model as a function of the frequency, the incident power intensity, and the type of

source. The phantom models are constructed of hollow forms consisting of styrofoam or thin fiberglass walls filled with synthetic tissue with dielectric properties similar to those of actual human tissue. The model is designed to be separated along any internal plane so that the SAR patterns may be quantified over that region of the model. The intact model is first exposed to the source for a sufficient period of time so that the synthetic material can increase in temperature according to the pattern of energy absorption. The model is then separated, and the two-dimensional temperature distribution is recorded by means of a thermograph camera and compared with that of a similar scan made before exposure. Difference in temperatures at each point on the model before and after exposure is used for computation of the SAR in watts per kilogram.

In a second method involving point-by-point measurements in the model, a microwave transparent temperature sensor is used. The temperature sensor is placed in a particular point in the model where the SAR measurement is to be made. The model is then exposed and the rate of change in temperature rise with time is noted and used for calculation of the SAR at that particular point.

Finally, a third method involves direct measurement of electric fields in the tissue with an implantable electric field sensor. From the known conductivity and the density of the synthetic tissue at that point, the measured electric field can be used for calculating the SAR.

The first two methods mentioned above require very high exposure fields, generally several orders of magnitude higher than the levels the subjects would normally be exposed to, but the third method necessitates relatively low exposure levels. For this project, however, it was felt that the first and second methods would provide the most information for conditions where the exposure fields were high, and the third method would be necessary where exposure fields were low, such as inside the automobile. The exposure fields necessary for the first method required that the UHF mobile antennas be redesigned so that they could function with up to 1,000 times more input power level than the mobile antenna normally needs. Then, a number of tests had to be made for verification of similarity between the

near-zone and radiation fields from the antennas and those of actual antennas used for UHF mobile communication.

In this work, the SAR was quantified for several forms of human subjects, including men, women, and children, exposed to both roof- and trunk-mounted mobile antennas. Because the tests were to be performed in a laboratory setting, the body of a 1971 Mazda 1200 automobile was designed so that it could be disassembled into parts that could easily be transported to a large, shielded anechoic chamber. The parts were thus reassembled into an intact unit simulating an actual car with its body at a proper distance above the floor of the chamber.

A 10-kW klystron amplifier provided sufficient energy to the mobile antennas for accurate determination of SAR by the thermograph and temperature-probe methods. For most locations of the model inside the car there was not sufficient energy coupling to enable thermal determination of the SAR, so the implanted electric field sensor was used in these instances. All of the measured SAR values were normalized to 1-W input power to the antennas. Measurements were made for the models spaced at varying distances from the antenna both inside and outside of the car.

In the following chapters all phases of the research are discussed in detail. Chapter 2 discusses the technical approach--the design of the phantom models, modification of the antennas, measurement methodology, and calibration techniques. Chapter 3 describes the experimental results for the man, woman, and child models obtained by thermography, temperature probes, and the electric-field sensor. This chapter also describes the patterns of the electric field, both inside and outside of the automobile. Finally, Chapter 4 covers the conclusions arrived at, the significance of the results in terms of both occupational and general-public safety standards, as well as the recommendations for future research.

2 TECHNICAL APPROACH

Automobile-Exposure Chamber and Radio Frequency Source

Since the objective of this research was to determine the SAR induced in human models by radiation from UHF mobile antennas, it was necessary to model as closely as possible the electromagnetic fields of a UHF antenna mounted on an automobile. A 1971 Mazda 1200 automobile body was chosen as the vehicle for testing the mobile antennas. The body shown in Fig. 1 was designed so that it could be disassembled for transportation and storage, but quickly reassembled for test requirements. The tests were conducted in the large anoechic chamber (12' x 12' x 24') of the Bioelectromagnetics Research Laboratory (BEMRL), with physical construction as shown in Fig. 2. The absorbing material was removed from the floor in the shielded room so that the automobile body could be placed at the proper distance above a perfectly conducting ground plane to represent the most conductive ground condition. The antennas to be tested consisted of a roof-mounted antenna shown at the left of Fig. 3, and a trunk-mounted antenna shown at the right of Fig. 3. For normal operation, the antennas were designed to function with 3- to 10-W input power in the 825- to 845-MHz frequency band. In Fig. 4 the automobile is shown in the shielded room with the roof-mounted receiving and transmitting antennas in place. One of the two identical antennas is connected to a receiver and the other to a transmitter. With the receiving antenna connected to a 50-ohm load, the voltage standing wave ratio (VSWR) of the transmitting antenna was determined and the power density at a point approximately 1 m away was measured. We used this information to design a similar antenna capable of handling up to 10-kW input power, necessary for performing the thermographic studies.

The high-powered transmitting antennas were fed by a Federal Communication Laboratory 10-kW klystron amplifier operating at a frequency of 835-MHz, the midfrequency of the automobile antenna. The klystron amplifier is shown in Fig. 5.

Fig. 1. Modification of automobile body for UHF antenna tests.

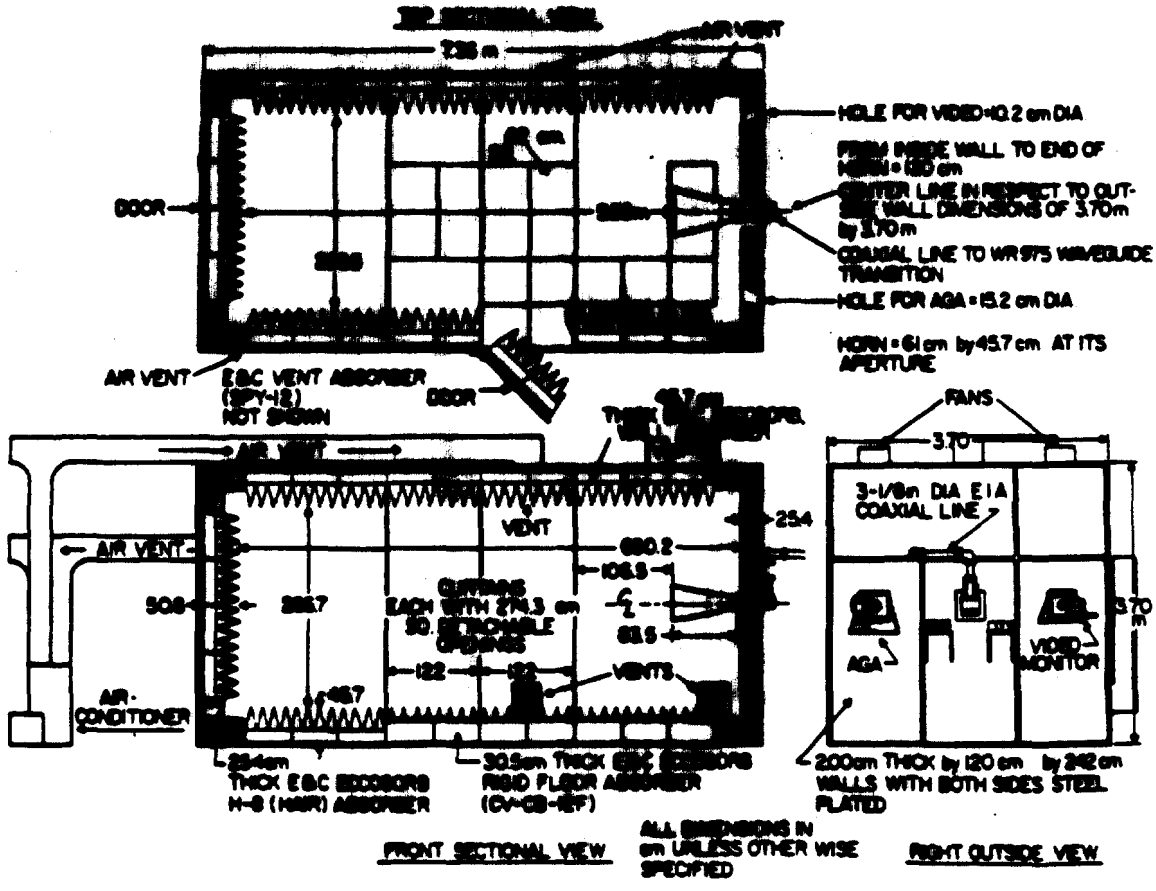

Fig. 2. Schematic of BEMRL anechoic exposure chamber.

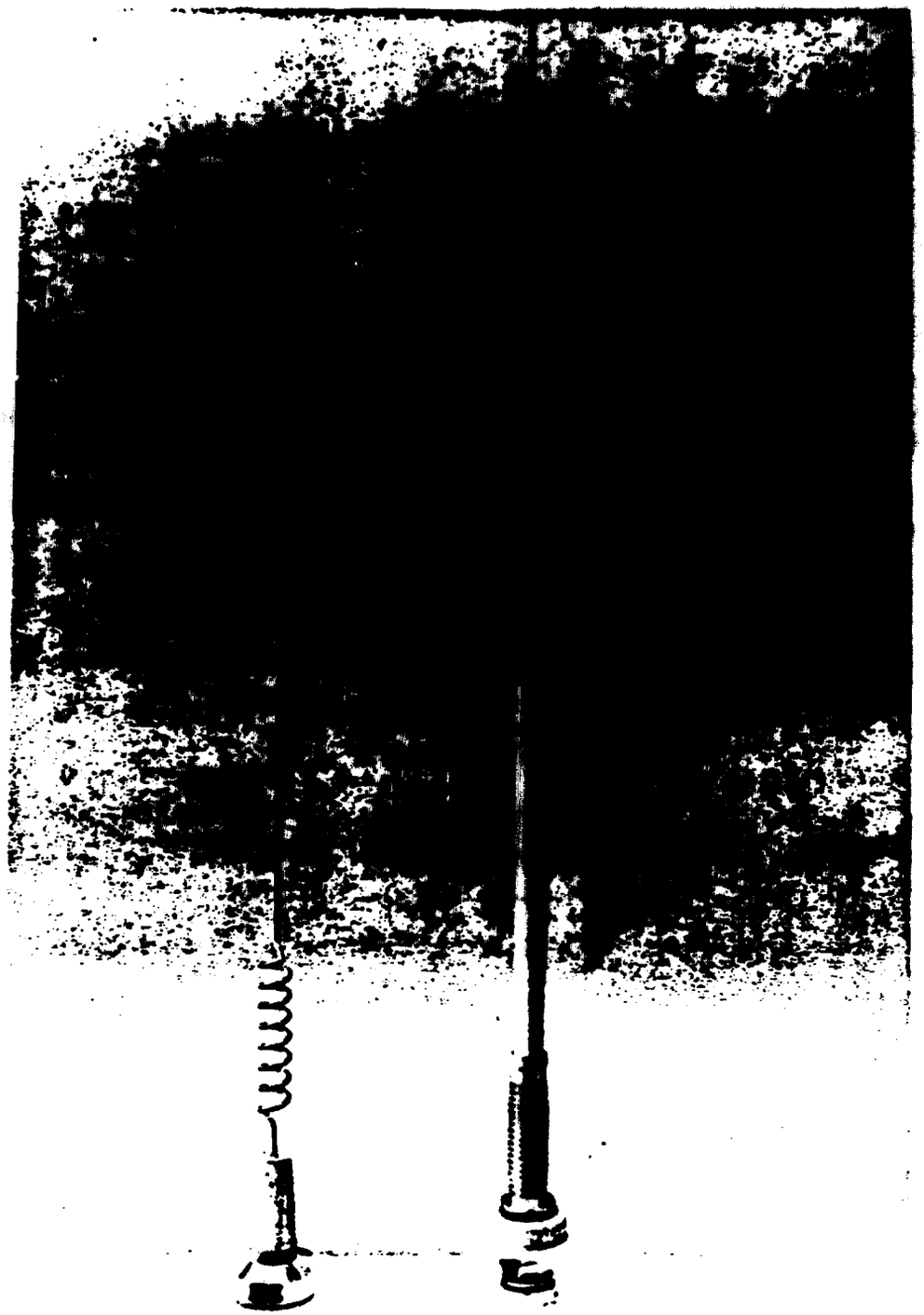

Fig. 3. Original Bell Laboratories roof-mounted antenna (left) and trunk-mounted antenna (right).